

# Delta-like factor 1 negatively regulates angiogenesis as a target gene of miR-126-5p after indirect revascularization surgery in patients with moyamoya disease



Yang Yang<sup>1</sup>, Cong Ling<sup>2</sup>, Shuangqi Gao<sup>2</sup>, Chao Li<sup>3</sup>, Robin Bhattarai<sup>4</sup>, Hui Wang<sup>2</sup>, Chuan Chen<sup>2</sup>

<sup>1</sup>Department of Radiology, Third Affiliated Hospital of Sun Yat-sen University, No. 600 Tianhe Road, Guangzhou 510630, Guangdong, PR China, <sup>2</sup>Department of Neurosurgery, Third Affiliated Hospital of Sun Yat-sen University, No. 600 Tianhe Road, Guangzhou 510630, Guangdong, PR China, <sup>3</sup>Department of Rehabilitation, Third Affiliated Hospital of Sun Yat-sen University, No. 600 Tianhe Road, Guangzhou 510630, Guangdong, PR China, <sup>4</sup>Department of Neurosurgery, B and C Medical College Teaching Hospital and Research Center, Birtamode, Jhapa, Nepal.

Date of submission: 1<sup>st</sup> March 2022

Date of acceptance: 6<sup>th</sup> June 2022

Date of publication: 25<sup>th</sup> June 2022

## Abstract

Promoting endothelial cell (EC) proliferation and angiogenesis after indirect revascularization surgery is crucial for decreasing the stroke rate in moyamoya patients. However, the role of delta-like factor 1 (DLK1) in regulating EC proliferation in chronically ischaemic brains and the specific mechanisms remain unclear. Therefore, we compared the expression levels of DLK1 in the dura mater (DM) tissues of patients with moyamoya disease and patients with aneurysms, and dual luciferase reporter and RNA binding protein immunoprecipitation assays were conducted to determine whether DLK1 is a target gene of miR-126-5p. The effect of DLK1 on EC proliferation and the interaction between DLK1 and miR-126-5p were explored in vitro. Then, we established an animal model of two-vessel occlusion together with encephalo-myo-synangiosis (2VO+EMS). The temporalis muscles (TMs) of the animals were transfected with DLK1 lentiviral RNA (Lv-DLK1) and short hairpin RNA (sh-DLK1) to compare the DLK1 expression, angiogenesis (CD31 count), and numbers of vacuoles and impaired tight junctions in the ECs of TM-covered chronically ischaemic brains as well as the cognitive improvement in each group. DLK1 expression was lower in the DM tissues of moyamoya patients than in those of the aneurysm patients, and DLK1 was identified as a target gene of miR-126-5p. In vitro, DLK1 inhibited EC proliferation, migration and angiogenesis and exerted effects opposite those of miR-126-5p. In 2VO+EMS rats, compared to the control transfection, the TM transfection of Lv-DLK1 induced significantly higher DLK1 expression and worse angiogenesis in the TM-covered ischaemic brain as well as less extensive cognitive improvement, while the transfection of sh-DLK1 into the TM had the opposite effects. In summary, DLK1, a target gene of miR-126-5p, negatively regulates angiogenesis in chronically ischaemic brains and is expected to be a new target to improve the efficacy of indirect revascularization surgery and the prognosis of moyamoya patients.

**Key words:** Delta-like factor 1, angiogenesis, indirect anastomosis formation, moyamoya disease, stroke, miR-126-5p.

## Access this article online

Website: <https://www.nepjol.info/index.php/NJN>

DOI: <https://doi.org/10.3126/njn.v19i2.43886>

## HOW TO CITE

Yang Y, Ling C, Gao S, Li C, Bhattarai R, Wang H, & Chen C. Delta-like factor 1 negatively regulates angiogenesis as a target gene of miR-126-5p after indirect revascularization surgery in patients with moyamoya disease. *NJNS*. 2022;19(2):3-16.



## Address for correspondence:

Chuan Chen

Department of Neurosurgery, Third Affiliated Hospital of Sun Yat-sen University, No. 600 Tianhe Road, Guangzhou 510630, Guangdong, PR China

E-mail: [chenchn6@mail.sysu.edu.cn](mailto:chenchn6@mail.sysu.edu.cn)

Copyright © 2022 Nepalese Society of Neurosurgeons (NESON)

ISSN: 1813-1948 (Print), 1813-1956 (Online)

## Introduction

Moyamoya disease, a congenital neurovascular disease, is one of the main causes of stroke<sup>1, 2</sup>. Indirect revascularization surgery, which can promote endothelial cell (EC) proliferation and angiogenesis in chronically ischaemic brains, is a routine and effective treatment method for patients with moyamoya disease<sup>3, 4</sup>. Indirect revascularization surgery is performed on patients with moyamoya disease to directly cover vascular-rich tissues (such as the dura mater [DM], temporalis muscle [TM]) on the ischaemic brain surface to promote the gradual



This work is licensed under a Creative Commons Attribution-Non Commercial 4.0 International License.

extension of newly formed capillaries from the DM (or TM) to the ischaemic brain tissue and thereby improve cerebral blood perfusion and prevent stroke. However, nearly half of adult moyamoya patients show poor potential for EC proliferation and angiogenesis, and this inadequate potential eventually leads to insufficient indirect anastomosis formation and poor clinical outcomes<sup>5</sup>. In this situation, promoting EC proliferation and angiogenesis is crucial for decreasing the stroke rate and improving clinical outcomes. However, specific strategies for promoting EC proliferation remain unclear.

Delta-like factor 1 (DLK1) is encoded by a paternally imprinted gene on human chromosome 14 and mouse chromosome 12 and is highly expressed during embryonic development<sup>6</sup>. DLK1 is synthesized as a membrane-bound precursor that has a signal peptide, six epidermal growth factor (EGF)-like extracellular repeats, a juxta-membrane region and a short intracellular tail<sup>7</sup>. Numerous studies have demonstrated that DLK1 plays a regulatory role in a series of mesoderm differentiation processes, including adipogenesis, myogenesis and osteoblastogenesis<sup>8</sup>. However, a few reports recently suggested that DLK1 negatively regulates EC proliferation<sup>9</sup>. Given that 1) both our previous study and studies from other scholars demonstrated that microRNA-126-5p (miR-126-5p) promotes EC proliferation<sup>10-12</sup>, 2) bioinformatics analysis (both TargetScan and miRDB) indicated the existence of a potential binding site between miR-126-5p and DLK1, and 3) a relatively authoritative study suggested that miR-126-5p and DLK1 interact<sup>13</sup>, we hypothesized that DLK1 inhibits EC proliferation and angiogenesis in patients with moyamoya disease as a target gene of miR-126-5p. However, further exploration is needed to reach a definite conclusion.

In addition, endothelial nitric oxide synthase (eNOS) produces nitric oxide to help regulate vascular function and participates in the regulation of EC repair and proliferation<sup>14</sup>. Our previous study suggested that eNOS exerts biological functions downstream of miR-126-5p; however, its expression level is positively correlated with that of miR-126-5p<sup>10</sup>. Therefore, considering that DLK1 could be a target gene of miR-126-5p, we presume that DLK1 serves as the in-between factor to directly regulate the expression of eNOS. However, the underlying regulatory pattern of DLK1 and eNOS remains unknown.

Therefore, this study aimed to explore the effect of DLK1 on EC proliferation and angiogenesis. Additionally, possible associations between DLK1 and miR-126-5p and between DLK1 and eNOS were investigated. The study findings are expected to provide new insight into strategies for promoting indirect anastomosis formation after indirect revascularization surgery and to further improve the prognosis of patients with moyamoya disease.

## Materials and methods

*Collection of DM tissues from patients with moyamoya disease and aneurysms.* First, we compared the DLK1 expression in DM tissues from patient with moyamoya disease (n = 8) and unruptured aneurysms (n = 8, control group). DM samples (1.0 × 0.5 cm) were collected from patients with moyamoya disease during revascularization procedures. DM samples were harvested from the temporal part of the head and stored for further use. All fresh samples were used for quantitative real-time polymerase chain reaction (qRT-PCR), frozen in liquid nitrogen and stored at -80°C. DM samples were also harvested from aneurysm patients undergoing clipping procedures, and the miR-126-5p expression in these samples was used as the control. The study was conducted in accordance with the Declaration of Helsinki (2000) and was approved by the Ethics Committee of the Third Affiliated Hospital of Sun Yat-sen University (no. [2019]06-440-13). Written informed consent was obtained from all the participants.

*Cell culture and grouping.* Human umbilical vein endothelial cells (HUVECs, cell lines; cat. no. CRL-1730) were purchased from the American Type Culture Collection. The cells were routinely cultured in a 5% CO<sub>2</sub> incubator at 37°C in M200 medium containing 2% FBS. HUVECs between passages 3 and 6 were used in all experiments. To investigate the regulatory effect of DLK1 on EC proliferation, we divided HUVECs into following subgroups, 1) control: naïve; 2) lentivirus negative control (Lv-NC): HUVECs transfected with a negative control lentivirus; 3) Lv-DLK1: HUVECs transfected with a DLK1 overexpression lentivirus; 4) short hairpin negative control (sh-NC): HUVECs transfected with a short hairpin RNA negative control lentivirus; 5) sh-DLK1: HUVECs transfected with a DLK1 short hairpin RNA lentivirus, and 6) sh-DLK1 + N<sup>G</sup>-nitro-L-arginine methyl ester (sh-DLK1+L-NAME): HUVECs transfected with both a DLK1 short hairpin RNA lentivirus and L-NAME (100 µmol/L, Invitrogen, Guangzhou, China). To investigate the interaction between miR-126-5p and DLK1 during EC proliferation, we divided HUVECs into the following subgroups, 1) control: naïve; 2) mimic NC: HUVECs transfected with 50 nM mimic negative control; 3) mimic: HUVECs transfected with 50 nM miRNA-126-5p mimic; 4) Lv-DLK1 + mimic: HUVECs transfected with a DLK1 overexpression lentivirus and then with a miRNA-126-5p mimic; 5) inhibitor NC: HUVECs transfected with 100 nM inhibitor negative control; 6) inhibitor: HUVECs transfected with 100 nM miRNA-126-5p inhibitor; and 7) sh-DLK1 + inhibitor: HUVECs transfected with a DLK1 short hairpin RNA lentivirus and then with a miRNA-126-5p inhibitor

*Cell transfection.* HUVECs were collected at 80% confluence for transfections. To increase or decrease

DLK1 expression, HUVECs were transfected with Lv-DLK1 or sh-DLK1 (Wuhan, Hubei, China). To increase or decrease miR-126-5p expression, HUVECs were transfected with mimic NC, miR-126-5p mimic, miRNA negative control inhibitor (inhibitor NC), or miR-126-5p inhibitor (RiboBio, Guangzhou, China). HUVECs were transfected using Lipofectamine 2000 (Invitrogen, Guangzhou, China) according to the manufacturer's instructions.

**Lentivirus packaging and transduction.** Lentivirus vectors (Lv-DLK1 and sh-DLK1) constructed by GenePharma (Shanghai, China) were used to stably overexpress or knockdown DLK1 in HUVECs. HUVECs were transduced with Lv-DLK1 or sh-DLK1 and selected with puromycin (Invitrogen) for 2 weeks to obtain stable HUVEC lines.

**Quantitative PCR (qRT-PCR).** TRIzol reagent (Invitrogen, Guangzhou, China) was used to isolate total RNA from HUVECs or DM tissues, and the Advantage RT-for-PCR Kit (TaKaRa, Otsu, Japan) was used to perform reverse transcription with U6 serving as the endogenous control. The following primers (Invitrogen) were used in this study: DLK1, 5'-TGACAATGTTTGCAGGTGC-3' (forward) and 5'-CATCTCTATCACAGAGCTCCC-3' (reverse); miR-126-5p, 5'-CCGACACGGGAGACAATG-3' (forward) and 5'-TCTGGAAGTGAGCCAATGTG-3' (reverse); and U6, 5'-CTGTGCCCATCTACGAGGGCTAT-3' (forward) and 5'-TTTGATGTCACGCACGATTTCC-3' (reverse). Both melt curve analysis and gel electrophoresis were used to verify the specificity of the fluorescent signal. The  $2^{-\Delta\Delta CT}$  method was used to calculate relative gene expression levels. All experiments were performed in triplicate.

**Immunofluorescence.** Briefly, sections were fixed with 4% paraformaldehyde in phosphate-buffered saline (PBS) for 5 min at room temperature, permeabilized, and blocked for 30 min with 0.1% Triton X-100 and 1% bovine serum albumin. Then, the fixed sections were washed and incubated for 1 h with a primary antibody against DLK1 (1:50; Bioss, Beijing, China), CD31 (1:100; Santa Cruz Biotechnology, Dallas, TX, USA), or eNOS (1:200; Cell Signaling Technology). The sections were then washed three times with PBS and incubated with secondary antibodies. The samples were subsequently counterstained with 4',6-diamidino-2-phenylindole (DAPI, Beyotime Biotechnology, Shanghai, China) to visualize nuclei. The number of CD31-positive cells was used as an indicator of the proliferation and distribution of capillary ECs. The number of positively stained cells in five random visual fields ( $100 \mu\text{m} \times 100 \mu\text{m}$ ) was counted. All experiments were performed in triplicate.

**Western blotting (WB).** The total protein concentration in HUVEC lysates was measured with a BCA Protein Assay Kit (Invitrogen). Proteins were separated by 10%

sodium dodecyl sulfate-polyacrylamide electrophoresis, transferred onto a PVDF membrane (Beyotime), and blocked for 60 min at room temperature using 5% nonfat milk. Primary antibodies against DLK1 (1:1000; Bioss), eNOS (1:1000; Abcam, Cambridge, UK) and  $\beta$ -tubulin (1:1000; Sigma-Aldrich) were used in this study. The membranes were incubated for 1 h at room temperature with an HRP-conjugated goat anti-rabbit secondary antibody (1:5000; Abcam). ECL WB detection reagents (Sigma-Aldrich) were used for protein detection, and ImageJ software (Bethesda, MD, USA) was used to process all data.

**Cell viability.** The CCK-8 assay was used to evaluate HUVEC viability (Solarbio Science & Technology, Beijing, China). Briefly, HUVECs were seeded into 96-well plates at a density of  $1 \times 10^4$  cells/well. After the indicated treatments for 24, 48 and 72 h, 20  $\mu\text{L}$  of CCK-8 solution was added to each well, and the plates were incubated for 2 h. The optical density (OD) values at a wavelength of 450 nm were measured to determine HUVEC viability.

**Transwell migration assay.** Transwell assays were used to determine cell invasion<sup>15</sup>. HUVECs were suspended in serum-free DMEM and seeded in the Matrigel-coated upper chamber. The lower chamber was filled with medium supplemented with FBS. The HUVECs were allowed to migrate for 24 h and then stained with 0.1% crystal violet. Finally, the invaded HUVECs that adhered to the surface of the lower membrane were counted in 5 random microscopic fields of each well (200 $\times$  magnification).

**Tube formation assay.** A tube formation assay was conducted to assess the tube formation ability of HUVECs as previously described<sup>10,16</sup>. Briefly, HUVECs ( $4 \times 10^5$  cells) were added to each well of a 48-well plate that contained 200  $\mu\text{L}$  of Matrigel (BD Biosciences, San Jose, CA, USA) in 1 mL of complete medium. The plates were then incubated at 37°C for 6 h, and the degree of tube formation was quantified by counting the numbers of tubes and branch points in five random fields (100 $\times$  magnification).

**Scratch wound assay.** To assess cell migration in vitro, a scratch wound assay was conducted as previously described<sup>10,17</sup>. In brief, a confluent monolayer of HUVECs ( $1 \times 10^5$  cells/mL in a six-well plate) was wounded with a 200- $\mu\text{L}$  micropipette tip. After incubation for 24 or 48 h, the degree of wound closure was determined under an inverted phase contrast microscope. The wound width was determined using Image-Pro Plus software 5.1 (Media Cybernetics, Inc. Siler Spring, MD, USA) for quantitative assessments.

**Dual luciferase reporter assay.** Wild-type (WT) and mutant (MUT) DLK1 were separately inserted into the pmirGLO vector to construct the WT DLK1 and MUT DLK1 vectors, respectively. These constructs were cotransfected with the mimic NC or miR-126-5p mimic

into HEK293T cells with Lipofectamine 2000 transfection reagent (Thermo Fisher Scientific). The luciferase activity of the vectors was detected using a Dual-Luciferase Reporter Assay System (Promega, Madison, WI, USA). Firefly luciferase activity was normalized to that of Renilla in each sample.

**RNA binding protein immunoprecipitation (RIP) assay.** For the RIP assay, cells were rinsed with cold PBS and fixed with 1% formaldehyde for 10 min. The RIP assay was performed with the EZ-Magna RIP Kit (Millipore, Bedford, MA, USA) according to the manufacturer's instructions. RNA was immunoprecipitated with an antibody against AGO2 (Abcam) or negative control IgG (Abcam). qRT-PCR was conducted to detect coprecipitated DLK1 RNA.

**Animals and subgrouping.** Adult male Sprague–Dawley rats (250–320 g,  $287.3 \pm 12.5$  g on average) were purchased from the animal centre of Sun Yat-sen University, Guangzhou, China (certificate number for this batch of rats: 20210222Aazz069000174; license number of the animal center: SCXK(GUANGDONG)2017-0083). The animals were allowed to adapt to the environment for 7 days before the experiments. All animal treatments and experiments were approved by the Institutional Animal Ethics Committee of Sun Yat-sen University (no. [2020]04-270- 55) and conformed to the Guide for the Care and Use of Laboratory Animals of the National Institutes of Health (publication no. 80-23, revised 1996). The animal body weights and behaviours were monitored every other day. Humane endpoints were determined when the animals exhibited >20% weight loss, dehydration and loss of ability to ambulate. No animals presented signs of humane endpoints requiring immediate euthanasia. Cervical dislocation was used as the method of euthanasia, and the rats were anaesthetized via an intraperitoneal injection of 10% chloral hydrate (320 mg/kg) prior to cervical dislocation. No rats exhibited signs of peritonitis after the administration of 10% chloral hydrate. The rats were randomly assigned to the following groups (n = 14 in each group): normal saline (NS), Lv-NC, Lv-DLK1, sh-NC and sh-DLK1.

**2VO surgical procedure.** The 2VO rat model with bilateral common carotid artery (CCA) ligation is commonly used to provide chronically ischaemic brains similar to those of moyamoya patient<sup>18</sup>. The procedure for 2VO rat modelling was performed as previously described<sup>19</sup>. Briefly, rats were anaesthetized via an intraperitoneal injection of 10% chloral hydrate (320 mg/kg) and showed no obvious signs of peritonitis. Anaesthetized rats were placed on a heating pad to maintain their temperature at 37°C. After creating an incision in the middle of the neck, the right CCA was ligated with two 3-0 silk threads. After 7 days, a scalp incision was made along the midline, a burr hole was made with an electric drill in the right frontal region (0.8 mm posterior and 3.4 mm lateral to bregma),

and a device fixed with cyanoacrylate adhesives for the contact probe was placed. Subsequently, the left CCA was exposed and ligated by the same method. Animals in the 2VO sham group was subjected to the same procedure but without CCA ligation. Laser Doppler flowmetry was used to measure cerebral blood flow (CBF) before and after the procedure. The mean CBF values are expressed as percentages of the baseline value. Successful 2VO model establishment was indicated by a decrease in the CBF to approximately 30% of the baseline value before surgery.

**EMS surgical procedure.** The 2VO+EMS rat model is commonly used to investigate the regulatory mechanism of angiogenesis after EMS procedures in patients with moyamoya diseases<sup>20, 21</sup>. The procedure for encephalo-myo-synangiosis (EMS) rat modelling was performed as previously described<sup>19</sup>. Briefly, immediately after establishment of the 2VO model, we performed EMS on the left cerebral hemisphere. The rats were anaesthetized with isoflurane (3% for induction and 2% for maintenance) and mechanically ventilated to maintain respiration using a rodent ventilator (Harvard Apparatus). After opening the skin and TM, a piece of skull from the temporoparietal region with a diameter of approximately 4 mm was removed using a microdrill. The DM and arachnoid membrane were carefully opened with microforceps and 1-mL syringe needles without damaging the brain. The TM and DM were stitched together, and the skin was then sutured. We assessed the effects of DLK1 on EC proliferation and angiogenesis by comparing the CD31 expression, number of vacuoles in ECs, number of abnormal tight junctions (TJs) between ECs and cognitive function and improvement among the groups<sup>22, 23</sup>. TM-covered brain tissue at a depth of less than 1 mm was harvested for further analysis. **Transfection of the rat TMs.** To upregulate or downregulate DLK1 expression, an aliquot of Lv-DLK1 (20  $\mu$ l,  $1 \times 10^8$  TU/mL) or sh-DLK1 (20  $\mu$ l,  $1 \times 10^8$  TU/mL) was divided equally in fourths and injected into four sites of the TM with a Hamilton microinjector immediately after the DM was opened. The same dose was injected into animals in the Lv-NC and sh-NC groups. In the NS group, 20  $\mu$ L of 0.9% NaCl was injected into TM tissue as a control. The entire injection period lasted 30 s. The dose was based on the manufacturer's recommendation (GenePharma) with modification as reported for local injection<sup>24, 25</sup>.

**Transmission electron microscopy (TEM).** The vacuoles in ECs and TJs between ECs were observed by TEM analysis. In this assay, 1-mm<sup>3</sup> brain cortex blocks were fixed at 4°C with fresh TEM fixative. Then, the tissues were rinsed, embedded in paraffin, and cut into ultrathin sections (50–80 nm). Images were acquired with a JEOL JEM 1400 transmission electron microscope (JEOL, Peabody, MA) at 80 kV on a Gatan Ultrascan 1000 CCD (Gatan, Inc., Pleasanton, CA). Vacuolation of the endothelium was quantified by normalizing the number

of vacuoles (>100 nm diameter) to the circumference of the vascular endothelium. The proportion of abnormal TJs (TJs with intercellular space or discontinuousness) to total TJs in 30 random visual fields was calculated.

**Morris water maze (MWM) test.** The MWM test was used to analyse cognitive impairment and improvement<sup>26</sup>. Briefly, a circular pool with a diameter of 180 cm and a depth of 60 cm was filled with water to a depth of 30 cm. The water temperature was  $22 \pm 2^\circ\text{C}$ , and the pool was divided into four quadrants. During the training period, a hidden escape platform (10×10 cm) was placed in quadrant III at 1 cm below the water surface, and this platform was removed during the escape latency test after training. During training, the rats were allowed 60 s to find the hidden escape platform, and the latency to escape onto the platform and the escape route were recorded. If a rat failed, it was guided onto the platform with a stick, and its latency time was recorded as 60 s. The training was conducted twice a day for 4 days. The escape latency, swim speed, time spent in the target quadrant and number of platform crossing were analysed using a video surveillance system (SMART, Panlab SL, Barcelona, Spain).

**Statistical analysis.** Statistical Program for Social Science (SPSS) version 22.0 was used for all statistical analyses. The data are presented as the means  $\pm$  standard deviations (SDs). Regarding the background data of the enrolled patients, measurement data were analysed using one-way ANOVA, and enumeration data were analysed with Fisher's exact tests. The results were evaluated by the two-tailed unpaired Student's t test. Significance is noted as \* $P < 0.05$ , \*\* $P < 0.01$  or not significant (ns). Each experiment was performed in triplicate.

## Results

*DLK1 is downregulated in the DM of moyamoya patients and is a direct target gene of miR-126-5p.* From December 2019 to March 2020, eight patients (2 men and 6 women) with moyamoya disease and 8 patients (4 men and 4 women) with unruptured aneurysms were enrolled in this study. The mean age of the patients with moyamoya disease was 46.9 years (range, 31-60 years), and that of the patients with unruptured aneurysms was 53.8 years (range, 37-71 years). The onset symptoms of patients with moyamoya disease, which occurred within the previous six months, included transient ischaemic attacks (3/8), limb numbness (3/8), amaurosis fugax (1/8), and seizures (1/8). The preoperative modified Rankin Scale score was  $\leq 2$  points for all patients with moyamoya disease. According to the preoperative digital subtraction angiography results for 16 hemispheres, Suzuki grade III was noted in 68.75% (11 of 16) of the hemispheres, and Suzuki grade II was noted in the remaining hemispheres (5 of 16). In all eight moyamoya patients, we performed the same surgical procedures, which were STA-MCA bypass combined with

encephalo-myo-synangiosis and dural inversion. During the procedures, we did not harvest the part of the dura mater including the major branch of the middle meningeal artery. Regarding the patients with aneurysms (control group), seven were asymptomatic, and one patient suffered from aneurysm-unrelated dizziness. All aneurysms were detected by routine health examinations. Five aneurysms were located on middle cerebral arteries, and the other three were located on posterior communicating arteries. The baseline data of the enrolled patients are shown in Table I. DLK1 expression in DM tissues was compared between the patients with moyamoya disease and those with unruptured aneurysms (control group) to determine whether DLK1 plays a role in regulating angiogenesis. The DLK1 expression in DM tissues was significantly lower in moyamoya patients than in control patients ( $n = 8$ ,  $0.4627 \pm 0.1428$  vs.  $1.0086 \pm 0.0602$ ,  $P < 0.0001$ ) (Figure 1A-1D). Dual luciferase reporter assays of HEK293T cells were conducted to investigate the possible interaction between miR-126-5p and DLK1. The complementary sequences between miR-126-5p and the DLK1 3'-UTR were obtained by bioinformatics analysis (Figure 1E). Luciferase activity was significantly suppressed in HEK293T cells cotransfected with the miR-126-5p mimic and WT DLK1 reporter but not in those transfected with the MUT DLK1 reporter (Figure 1F). We conducted anti-AGO2 RIP assays of HUVECs transiently overexpressing miR-126-5p and found significant enrichment of DLK1 pull-down by AGO2 (Figure 1G).

DLK1 inhibits EC proliferation in vitro by inhibiting eNOS expression. Next, we investigated the effect of DLK1 on EC proliferation and downstream cytokines in vitro. CCK-8 assays showed that compared to that in the control group, HUVEC viability was significantly higher in the sh-DLK1 group ( $n = 3$ ,  $P < 0.0001$ ) and significantly lower in the Lv-DLK1 group ( $n = 3$ ,  $P = 0.0013$ ) (Figure 2A). The WB results showed that compared to that in the control group, DLK1 expression was significantly higher in the Lv-DLK1 group ( $n = 3$ ,  $P = 0.0001$ ) and significantly lower in the sh-DLK1 group ( $n = 3$ ,  $P < 0.0001$ ). However, the eNOS inhibitor L-NAME had no effect on DLK1 expression. Accordingly, eNOS expression was significantly lower in the Lv-DLK1 group than in the control group ( $n = 3$ ,  $P < 0.0001$ ) and significantly higher in the sh-DLK1 group than in the control group ( $n = 3$ ,  $P < 0.0001$ ). However, the increased eNOS expression induced by sh-DLK1 was downregulated by the eNOS inhibitor L-NAME (Figure 2B, 2C). We then performed tube formation, scratch wound and Transwell migration assays to evaluate the tube formation, proliferation and invasion abilities of HUVECs in each group. The results showed decreased tube formation, proliferation and invasion of HUVECs in the Lv-DLK1 group compared to the control group, whereas HUVECs in the sh-DLK1 group showed enhanced tube formation, proliferation and

invasion abilities compared to those of the control group. However, the enhanced tube formation, proliferation and invasion abilities induced by sh-DLK1 was offset by the eNOS inhibitor L-NAME (Figure 2D-2J). In short, the above results suggest that the DLK1/eNOS pathway plays an essential role in EC proliferation, migration and angiogenesis.

*DLK1 reverses the regulatory effect of miR-126-5p on EC proliferation, angiogenesis and migration.* We conducted the following experiments to further verify the interaction between miR-126-5p and DLK1. Using qRT-PCR and WB, we determined that Lv-DLK1 transfection significantly reversed the suppressive effect of the miR-126-5p mimic on DLK1 expression, while sh-DLK1 transfection significantly reversed the stimulatory effect of the miR-126-5p inhibitor on DLK1 expression. However, neither Lv-DLK1 nor sh-DLK1 affected miR-126-5p expression (Figure 3A-3C). CCK-8 assays revealed that HUVEC viability was significantly elevated by the miR-126-5p mimic, while this increase was blocked by Lv-DLK1 transfection. Moreover, HUVEC viability was significantly suppressed by the miR-126-5p inhibitor, and this effect was significantly reversed by sh-DLK1 transfection (Figure 3D). Accordingly, the tube formation and Transwell assay results demonstrated that decreasing DLK1 expression alleviated the repression of angiogenesis and migration by the miR-126-5p inhibitor, while increasing DLK1 expression significantly reversed the stimulation of angiogenesis and migration by the miR-126-5p mimic (Figure 3E-3I).

*DLK1 inhibits angiogenesis in the ischaemic brains of 2VO+EMS rats.* The schedule and procedures are shown in Figure 4A-4G. We previously verified the ability of

EMS to induce EC proliferation in the ischaemic brains of 2VO rats<sup>10,19</sup>. Thus, in this study, immunofluorescence and WB analyses were performed to observe DLK1, eNOS and CD31 expression in brain tissues after the injection of NS, Lv-DLK1, sh-DLK1 and NC into the TM. The DLK1 expression in the Lv-DLK1 group was significantly higher than that in the NS group ( $n = 8$ ,  $P = 0.0002$ ), while that in the sh-DLK1 group was significantly lower than that in the NS group ( $n = 8$ ,  $P = 0.0308$ ). However, this difference was presumably attributed to intracellular DLK1 expression rather than extracellular DLK1 expression. In other words, membrane-bound DLK1 was likely the function-dominant form during the inhibition of angiogenesis. In addition, the expression levels of both eNOS and CD31 were significantly lower in the Lv-DLK1 group and significantly higher in the sh-DLK1 group than in the NS group (Figure 4H-4M). The same expression pattern of the abovementioned cytokines was observed by WB analysis (Figure 4N, 4O). The number of vacuoles per 10 mm of vascular endothelium was significantly increased in the Lv-DLK1 group but decreased significantly in the sh-DLK1 group compared to the NS group. Additionally, compared with that in the NS group, the number of abnormal TJs was significantly lower in the sh-DLK1 group and significantly higher in the Lv-DLK1 group (Figure 5A-5C). Finally, the MWM test was performed to compare cognitive improvement among groups. Although no significant difference in motor function (represented by swim speed) were observed among the groups, the cognitive improvement in the sh-DLK1 group was significantly greater than that in the NS group. However, the cognitive improvement was not significantly different in the Lv-DLK1 and NS groups (Figure 5D-5H).

	Moyamoya patients (n=8)	Aneurysm patients (n=8)	P value
Age (years)	46.9±10.0	53.8±11.1	0.2135
Sex (male:female)	2:6	4:4	0.6084
Hypertension (%)	50.0 (4/8)	87.5 (7/8)	0.2821
T2DM (%)	25.0 (2/8)	67.5 (5/8)	0.3147
Smoking (%)	12.5 (1/8)	37.5 (3/8)	0.5692
Hyperlipidaemia (%)	12.5 (1/8)	25.0 (3/8)	0.5692
Side of surgery (left: right)	3:5	5:3	0.6193

T2DM: type 2 diabetes mellitus.

Table 1: Baseline data of the included patients

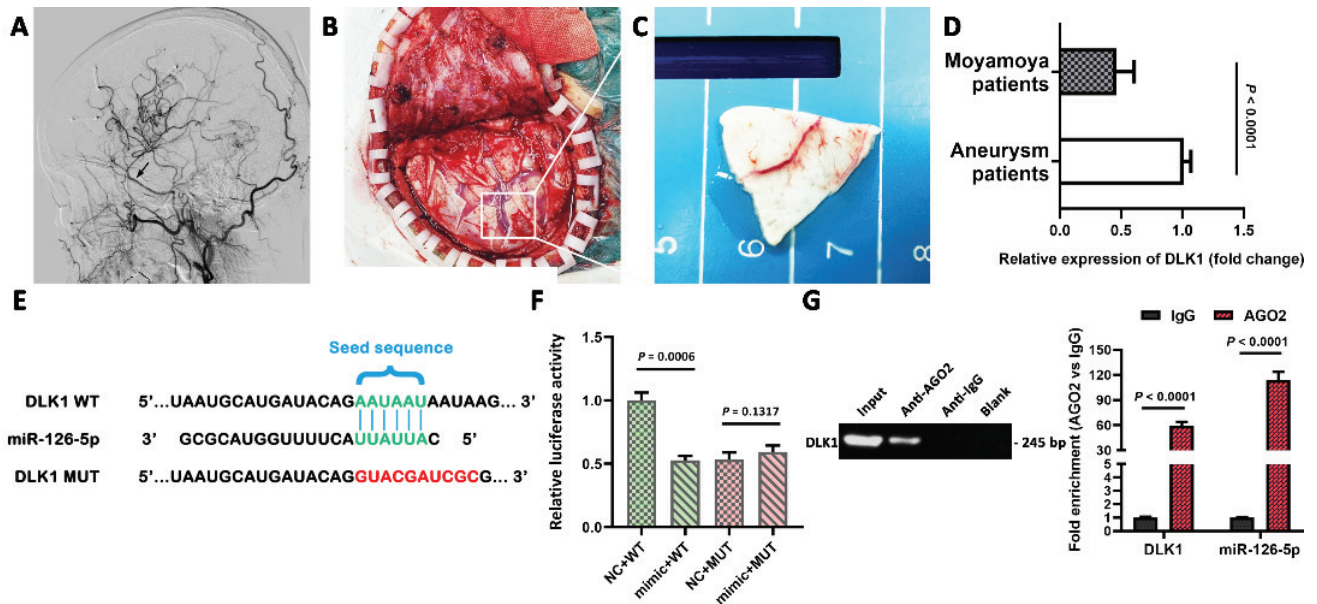


**Figure 1: Harvesting of clinical samples and the targeting relationship between miR-126-5p and DLK1.** (A) DSA film showing excellent anastomosis formation after indirect revascularization surgery in a moyamoya patient. The black arrow indicates the middle meningeal artery. (B) Intraoperative image showing the source of the DM sample. (C) The harvested DM sample. (D) Column chart showing the differences in miR-126-5p expression in DM samples from moyamoya patients ( $n = 8$ ) and aneurysm patients ( $n = 8$ ). (E) The predicted binding sites between miR-126-5p and DLK1. A mutation was introduced at the complementary miR-126-5p binding site in the DLK1 sequence. (F) Cotransfection of WT/MUT DLK1 and mimic NC/miR-126-5p mimic in HEK293T cells. (G) RIP assays were performed with an AGO2 antibody, followed by qPCR to enrich DLK1. DM: dura mater; NC: negative control; WT: wild-type; MUT: mutant.

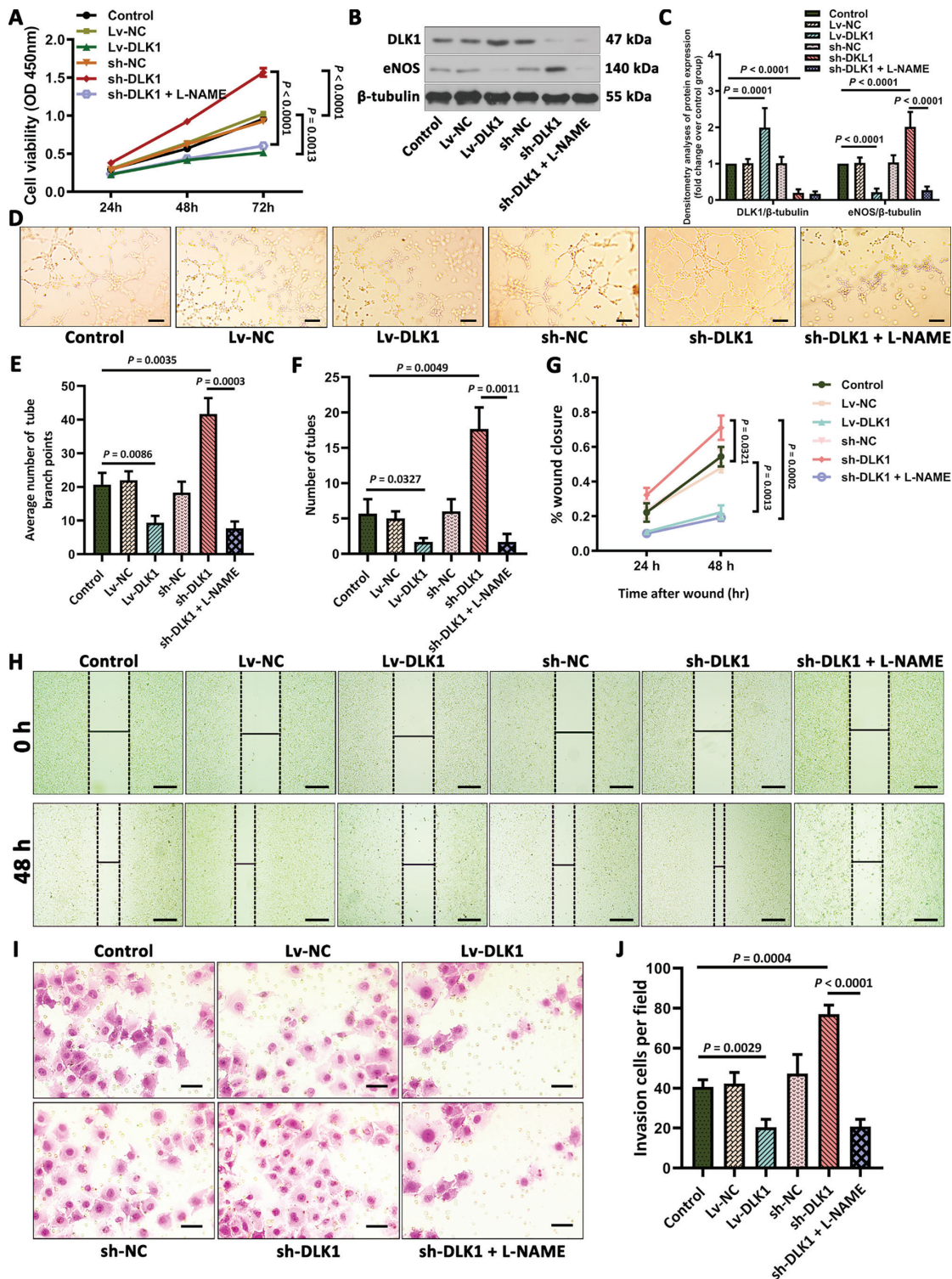


**Figure 2: DLK1 inhibits HUVEC migration and tube formation in vitro by inhibiting eNOS expression.** (A) Line graph showing the results of the CCK-8 assay of cell viability regarding the effect of DLK1 on HUVEC proliferation. (B) Representative western blot results showing the expression of DLK1 and eNOS in each group (normalized to the expression of β-tubulin). (C) Densitometry analyses of the western blot results. (D) Representative results of the tube formation assays in each group. Scale bar = 100 μm. (E) Quantification of the number of tubes. (F) Quantification of the average number of tube branch points. (G) Quantification of the scratch wound assay results at 24 and 48 h in each group. (H) Representative fields showing the scratch wound assay results at 48 h in each group. Scale bar = 200 μm. (I) Representative results of the Transwell migration assays in each group. Scale bar = 50 μm. (J) Quantification of the Transwell migration assay results. The data are representative images or are presented as the mean ± SD of n = 3 experiments.

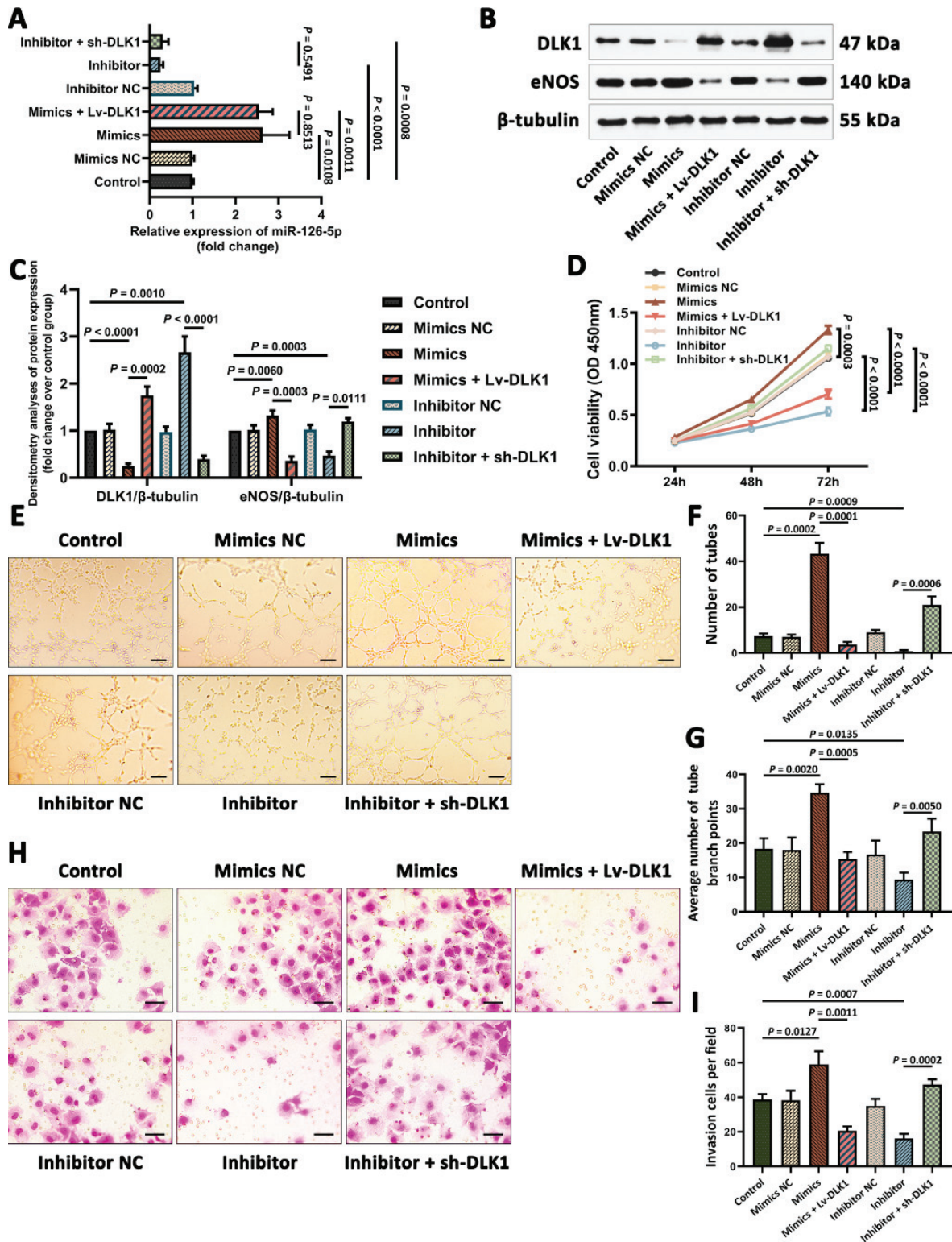


**Figure 3:** DLK1 reverses the proangiogenic effect of miR-126-5p in vitro. (A) qRT-PCR results showing the miR-126-5p expression in the different groups. (B) Representative western blot results showing the expression of DLK1 and eNOS in each group (normalized to the expression of  $\beta$ -tubulin). (C) Densitometry analyses of the DLK1 and eNOS expression in each group (normalized to  $\beta$ -tubulin expression). (D) Line graph showing the results of the CCK-8 assay of cell viability in each group. (E) Representative tube formation assay results in each group. Scale bar = 100  $\mu$ m. (F) Quantification of the number of tubes. (G) Quantification of the average number of tube branch points. (H) Representative Transwell migration assay results in each group. Scale bar = 50  $\mu$ m. (I) Quantification of the Transwell migration assay results. The data are representative images or are presented as the mean  $\pm$  SD of  $n = 3$  experiments.

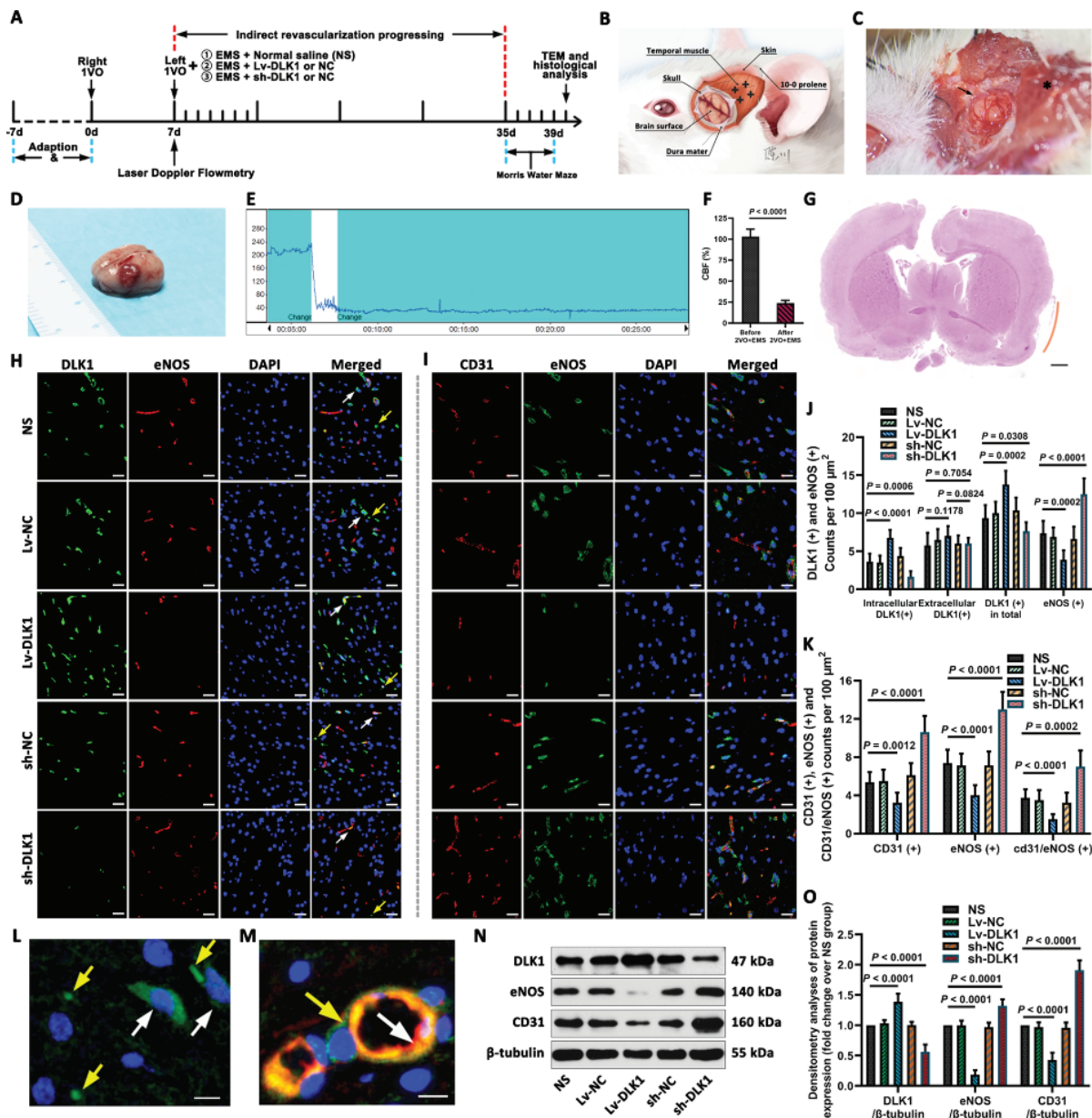


**Figure 4: DLK1 inhibits EC proliferation and angiogenesis in vivo.** (A) The schedule used to investigate the effects of the DLK1/eNOS pathway on angiogenesis in vivo. (B) Schematic drawing of the EMS procedure and the four sites of Lv-DLK1/sh-DLK1 injection into the TM. (C) Opening of the DM. The black asterisk indicates the TM, and the black arrow indicates the opened DM. (D) Brain samples (covered with the TM) from 2VO+EMS rats. (E) Representative graph of CBF changes before and after the 2VO procedure. (F) Doppler flowmetry results showing the CBF values before and after the 2VO procedure. (G) HE-stained slide of a brain from a 2VO+EMS rat. The red curve indicates the brain surface involved in EMS. Scale bar = 1 mm. (H) Immunofluorescence staining of cells positive for DLK1 and eNOS in the ischaemic brains of each group. The white arrow indicates intracellular DLK1+ staining, and the yellow arrow indicates extracellular DLK1+ staining. Scale bar = 20 μm. (I) Immunofluorescence staining of cells positive for CD31 and eNOS in the ischaemic brains of each group. (J) Quantitation of intracellular DLK1, extracellular DLK1, total DLK1 and eNOS positive cells in each group. (K) Quantitation of cells positive for CD31, eNOS and CD31/eNOS in each group. (L) Typical immunofluorescence staining showing intracellular DLK1 and extracellular DLK1 positivity. The white arrow indicates intracellular DLK1+ staining, and the yellow arrow indicates extracellular DLK1+ staining. Scale bar = 5 μm. (M) Typical dual immunofluorescence staining showing both CD31+ and eNOS+ cells. The white arrow indicates a CD31+ cell, and the yellow arrow indicates an eNOS+ cell. Scale bar = 5 μm. (N) Western blot results showing the expression of DLK1, eNOS and CD31 in each group. (O) Densitometry analyses of the above western blot results. The data are representative images or are presented as the mean ± SD. CBF: cerebral blood flow.

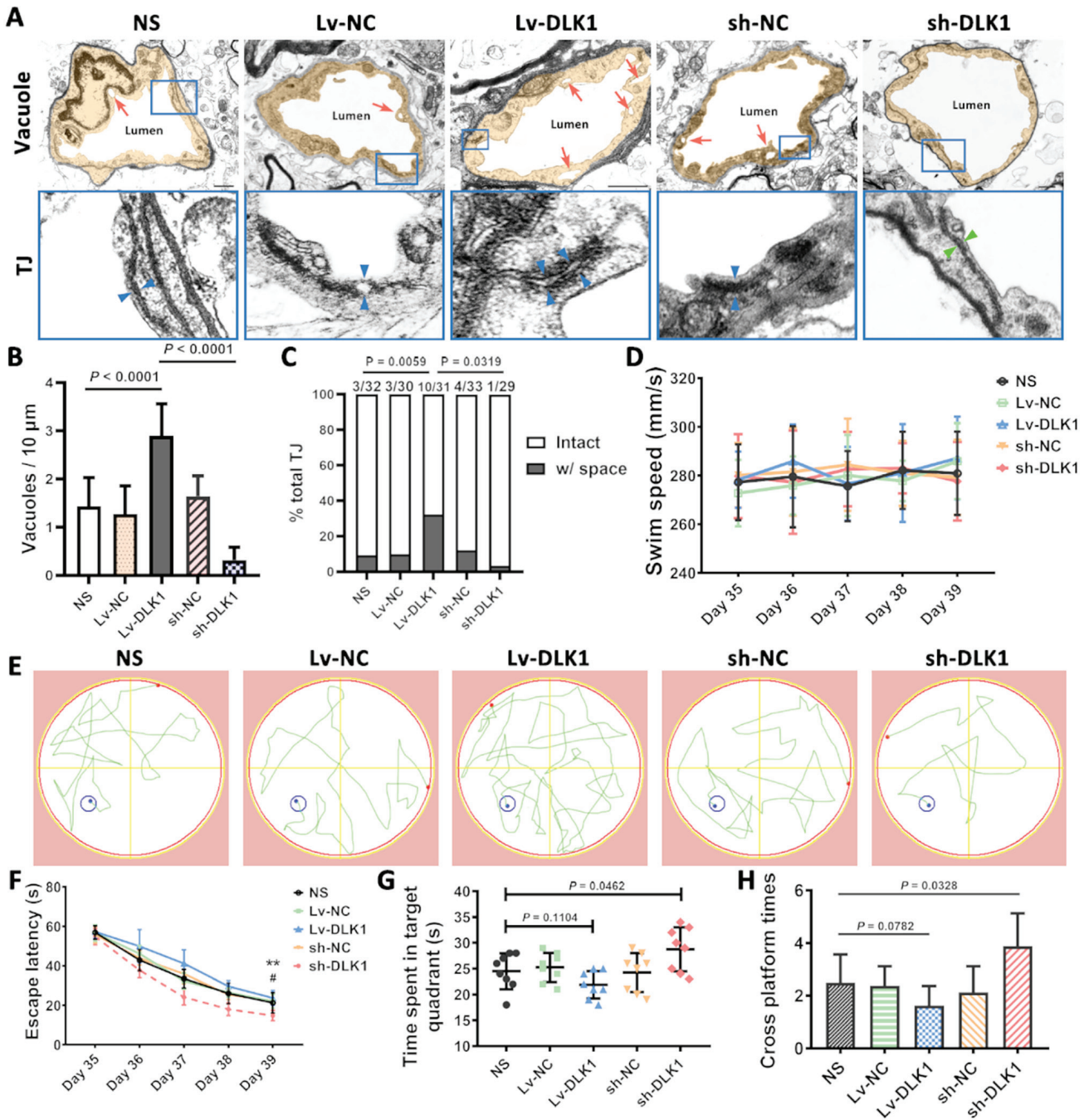


**Figure 5: TEM images of vacuoles and TJs and the MWM test results of each group.** (A) Representative TEM images of vacuoles and TJs in each group. Red arrows indicate vacuoles, green arrowheads indicate intact TJs, and blue arrowheads indicate abnormal TJs. Scale bar = 1  $\mu$ m. (B) Quantitation of the number of vacuoles per 10 mm of vascular endothelium in each group. (C) Quantitation of the abnormal TJs in each group. (D) Representative swimming paths of rats in each group. (E) Linear graph showing the escape latency of each group. #,  $P > 0.05$ , the antagonist group vs. the NS group; \*\*,  $P < 0.01$ , the agonist group vs. the NS group. (F) Time spent in the target quadrant for each group. (G) Linear graph showing the average swimming speed of each group. (H) Column graph showing the number of platform crossings for each group. The data are representative images or are presented as the mean  $\pm$  SD. MWM: Morris water maze.

## Discussion

*DLK1 plays an inhibitory role in angiogenesis in vitro.* DLK1, also known as Pref-1 and FA1, is a transmembrane glycoprotein belonging to the EGF superfamily<sup>27</sup>. Notably, recent studies have shown that DLK1 plays a critical role in angiogenesis<sup>13</sup>. In addition, the formation of extracranial-intracranial anastomosis derived from DM tissues is commonly observed in patients with moyamoya disease who have undergone indirect revascularization surgery<sup>28, 29</sup>. Therefore, the DLK1 expression levels in DM tissues were compared between patients with moyamoya disease and unruptured aneurysms (control group) to determine whether DLK1 participates in angiogenesis after indirect revascularization surgery. The qRT-PCR results showed that DLK1 was expressed at significantly lower levels in the DM of moyamoya patients than in that of unruptured aneurysm patients. Moreover, dual luciferase reporter and RIP assays revealed that DLK1 is a target gene of miR-126-5p, which was shown to promote EC proliferation in our previous study. These findings indicate that DLK1 may regulate anastomosis downstream of miR-126-5p in moyamoya patients. Next, in vitro EC experiments were conducted to confirm the biological effects of DLK1 on EC proliferation, migration and tube formation, as well as the interaction between DLK1 and miR-126-5p. The results showed that DLK1 had an inhibitory effect on EC proliferation, migration and tube formation downstream of miR-126-5p.

*DLK1 can negatively regulate anastomosis formation after indirect revascularization surgery.* We previously discovered that performing the EMS procedure on 2VO rats could successfully induce angiogenesis in the ischaemic brain covered by TM tissue (the same mechanism as the EMS effect on patients with moyamoya disease) and that the angiogenesis induced in the rats peaked in the 4th week after the EMS procedure<sup>19</sup>. Therefore, we used the 2VO+EMS rat model to determine whether DLK1 regulates angiogenesis in chronically ischaemic brains after indirect revascularization surgery (i.e., EMS). Four weeks after establishment of the rat model and TM transfection, TM-covered brain tissue was analysed; compared to the control group, the Lv-DLK1 group had significantly higher expression of DLK1 and significantly lower expression of both eNOS and CD31 (an EC marker). These in vivo expression patterns of the abovementioned cytokines were consistent with the in vitro findings regarding the DLK1/eNOS pathway. In addition, the TEM results revealed that DLK1 exerted a negative effect on EC repair and angiogenesis (more vacuoles and fewer intact TJs in the Lv-DLK1 group). Furthermore, the MWM test was performed to determine whether the increase in angiogenesis induced by DLK1 downregulation could improve the impaired cognitive function caused by

chronic ischaemia. The cognitive improvement in the sh-DLK1 group was significantly more extensive than that in the control group. Therefore, we can infer that the DLK1/eNOS pathway, which is downstream of miR-126-5p, negatively regulate anastomosis formation in the ischaemic brain after indirect revascularization surgery.

*Membrane-bound DLK1 is a dominant form that promotes angiogenesis.* DLK1 is synthesized as a membrane-bound precursor that has a signal peptide, six EGF-like extracellular repeats, a juxta-membrane region and a short intracellular tail<sup>30</sup>. DLK1 can function as either a membrane-bound or soluble protein, and these two forms likely have different biological functions<sup>27</sup>. Some studies have reported that soluble DLK1 promotes angiogenesis<sup>9</sup>, while others have reported that DLK1 inhibits angiogenesis<sup>31</sup>. In this study, we found that the DLK1 expression in brain tissue covered by Lv-DLK1-transfected TM (Lv-DLK1 group) was significantly higher than that in brain tissue covered by control-transfected TM, whereas angiogenesis was significantly inhibited in the Lv-DLK1 group compared to the control group. Additionally, the levels of both total DLK1 and membrane-bound DLK1 (intracellular DLK1) were significantly higher in the Lv-DLK1 group than in the control group. However, the levels of soluble DLK1 (extracellular DLK1) were not significantly different among the groups. Based on these data and the above results, we speculate that DLK1, acting downstream of miR-126-5p, inhibit angiogenesis in the ischaemic brain and that membrane-bound DLK1 is most likely the dominant functional form.

*Limitations.* First, cytokines downstream of DLK1 that promote angiogenesis other than eNOS need to be further studied. Second, the optimal dose for TM transfection in the 2VO+EMS rat model needs to be further explored. Third, the mechanism via which the effect of DLK1 extends from the TM to the ischaemic cortex remains unclear.

## Conclusion

Our novel results reveal that DLK1, a target gene of miR-126-5p, negatively regulates EC proliferation and angiogenesis and that downregulating DLK1 expression potentially promotes angiogenesis in chronically ischaemic brains. This finding provides a new target for promoting the formation of indirect anastomosis in patients undergoing indirect revascularization surgery, which is expected to help prevent the occurrence of stroke and improve the prognosis of moyamoya patients.

## Acknowledgements

We thank Liying Zhang for her expert technical assistance.

### Funding

This work was supported by the National Natural Science Foundation of China [grant no. 81901211], the Guangdong Basic and Applied Basic Research Foundation [grant no. 2019A1515010384], the Guangzhou Science and Technology Program [grant no. 202102010234], the Third Affiliated Hospital of Sun Yat-Sen University, Clinical Research Program [grant no. QHJH201908], and the Medical Science and Technology Research Foundation of Guangdong Province [grant no. A2019462]

### Ethics approval and consent to participate

The study was carried out in accordance with the Declaration of Helsinki (2000) and was approved by the Ethics Committee of the Third Affiliated Hospital of Sun Yat-sen University (no. [2019]06-440-13; no. [2020]04-270-55). Written informed consent was obtained from all the participants.

### Competing interests

The authors have no competing interests to declare.

### References

- Herve D, Ibos-Auge N, Calviere L, Rogan C, Labeyrie MA, Guichard JP, et al. Predictors of clinical or cerebral lesion progression in adult moyamoya angiopathy. *Neurology*. 2019;93(4):e388-e97. <https://doi.org/10.1212/WNL.00000000000007819>.
- Ando T, Shimada Y, Fujiwara S, Yoshida K, Kobayashi M, Kubo Y, et al. Revascularisation surgery improves cognition in adult patients with moyamoya disease. *J Neurol Neurosurg Psychiatry*. 2020;91(3):332-4. <https://doi.org/10.1136/jnnp-2019-321069>.
- Chen C, Wang H, Hou B, Luo L, Guo Y. Surgical Revascularization for Children with Moyamoya Disease: A New Modification to the Pial Syngangiosis. *World neurosurgery*. 2018;110:e203-e11. <https://doi.org/10.1016/j.wneu.2017.10.137>.
- Richards M, Grzenda A, Nelson E, Gitlin M. Psychiatric Comorbidity in Moyamoya Disease and Preliminary Guidelines For Treatment. *Am J Psychiatry*. 2019;176(4):269-74. <https://doi.org/10.1176/appi.ajp.2018.18040404>.
- Wang QN, Yang RM, Zou ZX, Wang XP, Zhang Q, Li DS, et al. Predictors of neoangiogenesis after indirect revascularisation in moyamoya disease: a 10-year follow-up study. *J Neurol Neurosurg Psychiatry*. 2021;92(12):1361-2. <https://doi.org/10.1136/jnnp-2020-325401>.
- Takagi H, Zhao S, Muto S, Yokouchi H, Nishihara H, Harada T, et al. Delta-like 1 homolog (DLK1) as a possible therapeutic target and its application to radioimmunotherapy using (125)I-labelled anti-DLK1 antibody in lung cancer models (HOT1801 and FIGHT004). *Lung Cancer*. 2021;153:134-42. <https://doi.org/10.1016/j.lungcan.2021.01.014>.
- Pittaway JFH, Lipsos C, Mariniello K, Guasti L. The role of delta-like non-canonical Notch ligand 1 (DLK1) in cancer. *Endocr Relat Cancer*. 2021;28(12):R271-R87. <https://doi.org/10.1530/ERC-21-0208>.
- Ichinose M, Suzuki N, Wang T, Wright JA, Lannagan TRM, Vrbanac L, et al. Stromal DLK1 promotes proliferation and inhibits differentiation of the intestinal epithelium during development. *Am J Physiol Gastrointest Liver Physiol*. 2021;320(4):G506-G20. <https://doi.org/10.1152/ajpgi.00445.2020>.
- Huang CC, Kuo HM, Wu PC, Cheng SH, Chang TT, Chang YC, et al. Soluble delta-like 1 homolog (DLK1) stimulates angiogenesis through Notch1/Akt/eNOS signaling in endothelial cells. *Angiogenesis*. 2018;21(2):299-312. <https://doi.org/10.1007/s10456-018-9596-7>.
- Chen C, Ling C, Gong J, Li C, Zhang L, Gao S, et al. Increasing the expression of microRNA-126-5p in the temporal muscle can promote angiogenesis in the chronically ischemic brains of rats subjected to two-vessel occlusion plus encephalo-myo-synangiosis. *Aging (Albany NY)*. 2020;12(13):13234-54. <https://doi.org/10.18632/aging.103431>.
- Esser JS, Saretzki E, Pankratz F, Engert B, Grundmann S, Bode C, et al. Bone morphogenetic protein 4 regulates microRNAs miR-494 and miR-126-5p in control of endothelial cell function in angiogenesis. *Thromb Haemost*. 2017;117(4):734-49. <https://doi.org/10.1160/TH16-08-0643>.
- Villain G, Poissonnier L, Noueihed B, Bonfils G, Rivera JC, Chemtob S, et al. miR-126-5p promotes retinal endothelial cell survival through SetD5 regulation in neurons. *Development*. 2018;145(1). <https://doi.org/10.1242/dev.156232>.
- Schober A, Nazari-Jahantigh M, Wei Y, Bidzhekov K, Gremse F, Grommes J, et al. MicroRNA-126-5p promotes endothelial proliferation and limits atherosclerosis by suppressing Dlk1. *Nat Med*. 2014;20(4):368-76. <https://doi.org/10.1038/nm.3487>.
- Nguyen H, Koh JY, Li H, Islas-Robles A, Meda Venkata SP, Wang JM, et al. A novel imidazolinone metformin-methylglyoxal metabolite promotes endothelial cell angiogenesis via the eNOS/HIF-1alpha pathway. *FASEB J*. 2021;35(7):e21645. <https://doi.org/10.1096/fj.202002674RR>.
- Zhang Y, Liu J, Jia W, Tian X, Jiang P, Cheng Z, et al. AGEs/RAGE blockade downregulates Endothelin-1

- (ET-1), mitigating Human Umbilical Vein Endothelial Cells (HUVEC) injury in deep vein thrombosis (DVT). *Bioengineered*. 2021;12(1):1360-8. <https://doi.org/10.1080/21655979.2021.1917980>.
16. Charron PN, Garcia LM, Tahir I, Floreani RA. Bio-inspired green light crosslinked alginate-heparin hydrogels support HUVEC tube formation. *J Mech Behav Biomed Mater*. 2022;125:104932. <https://doi.org/10.1016/j.jmbbm.2021.104932>.
  17. Latifi-Navid H, Soheili ZS, Samiei S, Sadeghi M, Taghizadeh S, Pirmardan ER, et al. Network analysis and the impact of Afibercept on specific mediators of angiogenesis in HUVEC cells. *J Cell Mol Med*. 2021;25(17):8285-99. <https://doi.org/10.1111/jcmm.16778>.
  18. Nakamura M, Imai H, Konno K, Kubota C, Seki K, Puentes S, et al. Experimental investigation of encephalomyosynangiosis using gyrencephalic brain of the miniature pig: histopathological evaluation of dynamic reconstruction of vessels for functional anastomosis. Laboratory investigation. *J Neurosurg Pediatr*. 2009;3(6):488-95. <https://doi.org/10.3171/2008.6.PEDS0834>.
  19. Li W, Wei L, Wang B, Gao S, Huang T, Li Z, et al. The trend of indirect anastomosis formation in a 2-vessel occlusion plus encephalo-myo-synangiosis rat model. *Ann Transl Med*. 2021;9(1):19. <https://doi.org/10.21037/atm-20-2936>.
  20. Hecht N, Pena-Tapia P, Vinci M, von Degenfeld G, Woitzik J, Vajkoczy P. Myoblast-mediated gene therapy via encephalomyosynangiosis--a novel strategy for local delivery of gene products to the brain surface. *J Neurosci Methods*. 2011;201(1):61-6. <https://doi.org/10.1016/j.jneumeth.2011.07.011>.
  21. Kim HS, Lee HJ, Yeu IS, Yi JS, Yang JH, Lee IW. The neovascularization effect of bone marrow stromal cells in temporal muscle after encephalomyosynangiosis in chronic cerebral ischemic rats. *Journal of Korean Neurosurgical Society*. 2008;44(4):249-55. <https://doi.org/10.3340/jkns.2008.44.4.249>.
  22. Nahirney PC, Reeson P, Brown CE. Ultrastructural analysis of blood-brain barrier breakdown in the peri-infarct zone in young adult and aged mice. *J Cereb Blood Flow Metab*. 2016;36(2):413-25. <https://doi.org/10.1177/0271678X15608396>.
  23. Xu J, Long H, Chen W, Cheng X, Yu H, Huang Y, et al. Ultrastructural Features of Neurovascular Units in a Rat Model of Chronic Compressive Spinal Cord Injury. *Front Neuroanat*. 2017;11:136. <https://doi.org/10.3389/fnana.2017.00136>.
  24. Deng SL, Zhu J, Huang Q, Fu WL, Li Q, Chen G, et al. Lentiviral vector-mediated shRNAs targeting a functional isoform of the leptin receptor (Ob-Rb) inhibit cartilage degeneration in a rat model of osteoarthritis. *Osteoarthritis Cartilage*. 2017;25(11):1912-21. <https://doi.org/10.1016/j.joca.2017.08.003>.
  25. Tasfaout H, Lionello VM, Kretz C, Koebel P, Messaddeq N, Bitz D, et al. Single Intramuscular Injection of AAV-shRNA Reduces DNM2 and Prevents Myotubular Myopathy in Mice. *Mol Ther*. 2018;26(4):1082-92. <https://doi.org/10.1016/j.ymthe.2018.02.008>.
  26. D'Hooge R, De Deyn PP. Applications of the Morris water maze in the study of learning and memory. *Brain Res Brain Res Rev*. 2001;36(1):60-90. [https://doi.org/10.1016/S0165-0173\(01\)00067-4](https://doi.org/10.1016/S0165-0173(01)00067-4).
  27. Grassi ES, Jeannot P, Pantazopoulou V, Berg TJ, Pietras A. Niche-derived soluble DLK1 promotes glioma growth. *Neoplasia*. 2020;22(12):689-701. <https://doi.org/10.1016/j.neo.2020.10.005>.
  28. Hara S, Nariai T, Inaji M, Tanaka Y, Maehara T. Imaging Pattern and the Mechanisms of Postoperative Infarction After Indirect Revascularization in Patients with Moyamoya Disease. *World neurosurgery*. 2021;155:e510-e21. <https://doi.org/10.1016/j.wneu.2021.08.098>.
  29. Fiaschi P, Scala M, Piatelli G, Tortora D, Secci F, Cama A, et al. Limits and pitfalls of indirect revascularization in moyamoya disease and syndrome. *Neurosurgical review*. 2021;44(4):1877-87. <https://doi.org/10.1007/s10143-020-01393-1>.
  30. Grassi ES, Pietras A. Emerging Roles of DLK1 in the Stem Cell Niche and Cancer Stemness. *J Histochem Cytochem*. 2022;70(1):17-28. <https://doi.org/10.1369/00221554211048951>.
  31. Rodriguez P, Higuera MA, Gonzalez-Rajal A, Alfranca A, Fierro-Fernandez M, Garcia-Fernandez RA, et al. The non-canonical NOTCH ligand DLK1 exhibits a novel vascular role as a strong inhibitor of angiogenesis. *Cardiovasc Res*. 2012;93(2):232-41. <https://doi.org/10.1093/cvr/cvr296>.